01 Jan 2020

Bridge Resilience Assessment with INSPIRE Data

Iris Tien

Yijian Zhang

FINAL REPORT

#INSPIRE-009

GRANT NO: 69A3551747126
GRANT PERIOD: 11/30/16 – 09/30/22
PROJECT PERIOD: 11/30/16 – 06/30/20

Inspecting and Preserving Infrastructure through Robotic Exploration (INSPIRE)

Tier 1 University Transportation Center Sponsored by the Office of the Assistant Secretary for Research and Technology (OST-R)

Project/Report Title:	**Bridge Resilience Assessment with INSPIRE Data**
Consortium Member:	Georgia Institute of Technology
Principal Investigator:	Iris Tien, Ph.D.
Co-Principal Investigator(s):	
Report Authors:	Iris Tien, Yijian Zhang

DISCLAIMER

The contents of this report reflect the views of the authors, who are responsible for the facts and the accuracy of the information presented herein. This document is disseminated in the interest of information exchange. The report is funded, partially or entirely, by a grant from the U.S. Department of Transportation's University Transportation Centers Program. However, the U.S. Government assumes no liability for the contents or use thereof.

TECHNICAL REPORT DOCUMENTATION PAGE

1. Report No. INSPIRE-009	**2. Government Accession No.** (blank)	**3. Recipient's Catalog No.** (blank)
4. Title and Subtitle Bridge Resilience Assessment with INSPIRE Data		**5. Report Date** 06/30/2020
		6. Performing Organization Code
7. Author(s) Iris Tien, Yijian Zhang		**8. Performing Organization Report No.**
9. Performing Organization Name and Address Georgia Institute of Technology 790 Atlantic Drive Atlanta, GA 30332-0355		**10. Work Unit No.** (blank)
		11. Contract or Grant No. USDOT #69A3551747126
12. Sponsoring Agency Name and Address Office of the Assistant Secretary for Research and Technology U.S. Department of Transportation 1200 New Jersey Avenue, SE Washington, DC 20590		**13. Type of Report and Period Covered** Final Report Period: 03/01/2017 – 06/30/2020
		14. Sponsoring Agency Code (blank)

15. Supplementary Notes
The investigation was conducted under the auspices of the INSPIRE University Transportation Center.

16. Abstract
This project proposed a methodology to assess the impact of corrosion on the performance of bridges. The combined analytical and numerical modeling of shear-critical and lap-spliced columns is detailed, and outcomes are verified with previous experimental test data. The impact of corrosion on risk is assessed through conducting fragility analyses. Results quantify the increase in failure probabilities of these structures, measured by increasing probabilities of exceeding defined damage states, with increasing levels of corrosion. Corrosion is found to have a larger impact on increasing probabilities of exceeding more severe damage states. Twenty percent mass loss of reinforcement increases the probability of exceeding the complete damage state by up to 49% and 34% for a shear-critical and lap-spliced column, respectively. The effect is more pronounced at intermediate loading intensities, where there is uncertainty about the performance of the structure. Comparing between failure modes, bridges with columns of short lap splice are more vulnerable to collapse under the same degree of corrosion compared with shear-critical columns.

17. Key Words Bridge, Corrosion, Inspection Data, Risk Assessment	**18. Distribution Statement** No restrictions	
19. Security Classification (of this report) Unclassified	**20. Security Classification (of this page)** Unclassified	**21. No of Pages** 34

Form DOT F 1700.7 (8-72) Reproduction of form and completed page is authorized.

EXECUTIVE SUMMARY

Increasing corrosion in aging reinforced concrete structures is increasing their vulnerability to failures. This is particularly true for bridges with low-ductility columns, including shear-critical columns and columns with short lap splices. In this project, a methodology to assess the impact of corrosion on performance of these structures is proposed. The combined analytical and numerical modeling of shear-critical and lap-spliced columns is detailed, and outcomes are verified with previous experimental test data. Corrosion effects are accounted for through reduction of longitudinal and transverse reinforcement and bond deterioration between the steel and concrete through corrosion-induced cracking. The impact of corrosion on risk is assessed through conducting fragility analyses. Results quantify the increase in failure probabilities of these structures, measured by increasing probabilities of exceeding defined damage states, with increasing levels of corrosion. Corrosion is found to have a larger impact on increasing probabilities of exceeding more severe damage states. Twenty percent mass loss of reinforcement increases the probability of exceeding the complete damage state by up to 49% and 34% for a shear-critical and lap-spliced column, respectively. The effect is more pronounced at intermediate loading intensities, where there is uncertainty about the performance of the structure. Comparing between failure modes, bridges with columns of short lap splice are more vulnerable to collapse under the same degree of corrosion compared with shear-critical columns.

ACKNOWLEDGMENT

Financial support for this INSPIRE UTC project was provided by the U.S. Department of Transportation, Office of the Assistant Secretary for Research and Technology (USDOT/OST-R) under Grant No. 69A3551747126 through INSPIRE University Transportation Center (http://inspire-utc.mst.edu) at Missouri University of Science and Technology. The views, opinions, findings, and conclusions reflected in this publication are solely those of the authors and do not represent the official policy or position of the USDOT/OST-R, or any State or other entity.

Table of Contents

1 MOTIVATION AND PROJECT OBJECTIVES 7

2 SHEAR-CRITICAL COLUMN CONSIDERING CORROSION EFFECT 9

2.1 Numerical model 9

2.2 Verification with experimental tests 10

2.3 Analytical modeling of corrosion effects 12

3 COLUMNS WITH SHORT LAP SPLICE CONSIDERING CORROSION EFFECT 17

3.1 Numerical model accounting for corrosion effects 18

3.2 Verification with experimental tests 20

4 SEISMIC FRAGILITY ASSESSMENT 22

4.1 Bridge parameters 22

4.2 Bridge risk assessment 25

5 CONCLUSIONS 31

6 REFERENCES 32

1 MOTIVATION AND PROJECT OBJECTIVES

Aging of bridge structural components due to natural degradation events, including corrosion, creates safety issues in the structural system and can lead to possible bridge failures. Collecting and analyzing inspection data provide a way to monitor and assess the safety condition of bridges. This project presents a new approach for risk assessment of bridges subject to corrosion based on collected corrosion inspection data. The research focuses on utilizing collected data to evaluate the bridges' structural conditions through fragility assessments.

As bridges across the U.S. continue to age, they are increasingly vulnerable to failures. Bridge column failures in flexure exhibit ductile behavior, a failure mechanism that is better understood and more predictable. In contrast, shear failure and pull-out failure of columns are often brittle and catastrophic, presenting a difficult problem for structural engineers to predict their behavior. These effects are particularly pronounced during seismic events and for structures designed with light transverse reinforcement and short lap splices. As a result, these bridge column types have high probability of undergoing brittle failure modes.

At the same time, deterioration of columns due to corrosion has become a critical problem for aging bridges, presenting not only significant costs for retrofitting, but also serious safety concerns under seismic conditions (Ghosh and Padgett, 2010; Choe et al., 2009). Previous studies have investigated the influence of pitting corrosion on the mechanical properties of corroded steel bars (Almusallam, 2001; Du et al., 2005; Apostolopoulos et al., 2006). Du et al. (2005) have studied the effect of corrosion damage on residual capacity and corroded bars' ductility to account for the impact of pitting corrosion on the constitutive behavior of reinforcement in tension. An investigation of spatial variability in corrosion patterns of corroded bars using 3D optical measurements has been conducted by Kashani et al. (2013).

They have found that the geometrical properties of corroded bars can be modeled using a lognormal distribution.

With more than one-fourth of bridges over 50 years old (FHWA, 2013), column design details in these aging bridges make them vulnerable to brittle failure modes as well as further deterioration due to corrosion. Few previous studies, however, have investigated different failure modes of columns and quantified the impact of corrosion in these cases. This project provides a methodology to account for deterioration due to corrosion focusing on predictions of performance for bridges with low-ductility column types. The analysis enables the quantification of the impact of corrosion on risk assessment of these bridges through predicted failure probabilities as a function of levels of corrosion for these structures.

2 SHEAR-CRITICAL COLUMN CONSIDERING CORROSION EFFECT

The objective in this work is to assess updates in bridge risk due to measured corrosion levels. Risk is measured using fragility functions. Fragility functions provide a way to quantify structural risks under varying loading intensities. Equation (1) represents the conditional probability of a structure exceeding a specific damage state DS given a realization y of intensity measure IM.

$$Fragility = Pr[DS|IM = y] \quad (1)$$

2.1 Numerical model

Both experimental research and post-earthquake data have shown that columns with widely spaced transverse reinforcement have a higher probability of failing in shear, leading to collapse of the system (Elwood, 2004). Widely spaced transverse reinforcement is a characteristic of many bridges built prior to the 1970s before the importance of transverse reinforcement was understood. In this section, a numerical model is established and used to assess bridge behavior. A calibrated shear spring element is adopted to capture shear degradation (LeBorgne, 2012) for simulation in OpenSees (McKenna et al., 1997). More specifically, the shear spring element can monitor forces and deformation in the beam-column element. Shear degradation is triggered by reaching either a limiting lateral force or a limiting plastic-hinge rotation capacity (LeBorgne and Ghannoum, 2013).

Figure 1 presents the numerical model with a double-curvature bridge column. Since the bridge column's boundary conditions are fixed at both the top and bottom in this selected bridge type, the inflection point approximately occurs at the bridge column's mid-span. A middle node is added to capture the displacement demand at the mid-span. Two force-based beam-column elements are in series with a zero-length shear spring element and a bond-slip element used to account for the strain penetration effect. The bond slip typically occurs along a portion of anchorage length (Zhao and Sritharan, 2007). Each

force-based beam-column element possesses four gauss integration points, which allows the model to capture the spread of plasticity along the column and fiber section consisting of uniaxial constitutive models for steel and concrete. A shear spring is added at the bottom end of the column to account for the effect of shear degradation in the case of shear failure mode. As the shear spring element is designed for a column with a rectangular cross section, the column's width and depth are taken as $0.89D$ adopted from ACI provisions (2011) and Liu et al. (2015), where D is the column diameter.

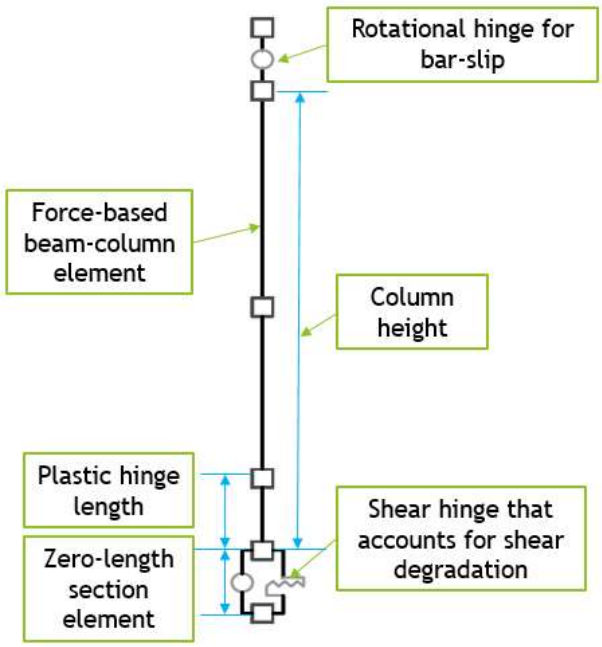

Figure 1. The numerical model for shear-critical column

2.2 Verification with experimental tests

Force-displacement curves from the model are compared to those from experimental tests of circular shear-critical columns conducted by Ang (1985) To verify the numerical model's accuracy. Experimental data on corroded shear-critical columns are not available, so results are compared with the pristine column. The two specimens for comparison have a diameter of 400 mm and a height of 600 mm.

Longitudinal reinforcement consists of 20 steel bars with a diameter of 16 mm, and transverse reinforcement consists of steel bars with a diameter of 6 mm at 60 mm and 80 mm spacing for the two specimens. Figure 2 shows both experimental and numerical results from static cyclic tests for each specimen.

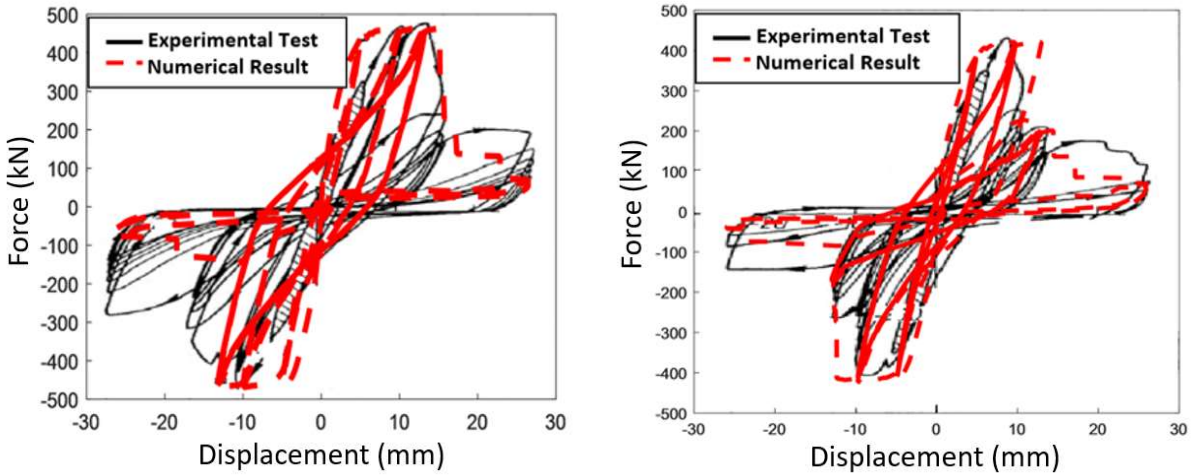

Figure 2. Force-displacement curves for specimens with (a) 60 mm and (b) 80 mm transverse reinforcement spacing from experimental tests (Ghee, 1985) and numerical models developed in this study

The solid line and dashed line represent experimental results and numerical results, respectively. From Figure 2, the numerical model can capture the force-displacement envelope, including the point where the specimen begins to lose its load-carrying resistance due to shear failure. Table 1 shows the percentage differences in the peak force and displacement corresponding with a 20% strength drop between the numerical and experimental results.

Table 1. Comparison between experimental tests and numerical model results for shear-critical column

	60 mm Transverse Spacing Specimen		80 mm Transverse Spacing Specimen	
	Peak Force (kN)	Displ. at 20% Strength Drop (mm)	Peak Force (kN)	Displ. at 20% Strength Drop (mm)
Experimental Test	462	15.1	468	10.1
Numerical Model	469	13.8	450	9.3
% Difference	1.6%	8.6%	3.8%	7.9%

From Table 1, the percentage differences for both specimens between the experimental and numerical results are less than 5% and 10% for the peak force and displacement corresponding with a 20% strength drop, respectively. Previous studies have investigated the effect of pitting corrosion on the mechanical properties of corroded steel bars (Almusallam, 2001; Du et al., 2005; Apostolopoulos et al., 2006). The effects of corrosion damage on residual capacity and the ductility of corroded bars are adopted in this study as in Du et al. (2005) to account for the effect of pitting corrosion on the constitutive behavior of reinforcement in tension. Kashani et al. (2013) have conducted 3D optical measurements of corroded bars to investigate spatial variability in corrosion patterns and found that corroded bars' geometrical properties can be modeled using a lognormal distribution. This study uses the lognormal distribution's mean values to account for pitting corrosion's impact on corroded bars' geometric properties. In other words, the influence of corrosion is accounted for in terms of the averaged response of the stress-strain behavior and the averaged reduced cross section of steel with uniform mass loss (Kashani et al., 2015; Kashani et al., 2016).

2.3 Analytical modeling of corrosion effects

To account for corrosion in the shear-critical column, both the strength limit curve and unloading stiffness are modified in the shear spring element. First, the strength limit curve is constructed following

Equation (2) provided in ASCE 41 (2007). The curve is then modified by considering the average reductions in diameter of reinforcement and yield strength as shown in Equations (3) and (4).

$$V_n = k\frac{A_v f_y d_b}{s} + \lambda k\left(\frac{6\sqrt{f_c'}}{\frac{M}{VD}}\sqrt{1+\frac{N_u}{6\sqrt{f_c'}A_g}}\right)0.8A_g \quad (2)$$

$$d_{b\_cor} = \frac{d_b}{10}\sqrt{100-\psi} \quad (3)$$

$$f_{y\_cor} = f_y(1-\beta\psi) \quad (4)$$

V_n is the lateral shear strength of the column and A_v is an area of transverse reinforcement. d_{b_cor} and d_b are the corroded and pristine diameter of either longitudinal or transverse steel bar, respectively, while f_{y_cor} and f_y are corroded and pristine yield strength of steel bar, respectively. s is spacing of transverse reinforcement, N_u is axial compression force, $\frac{M}{VD}$ is the largest ratio of a moment to shear times the effective depth, A_g is the gross cross-sectional area of the column, and f_c' is the compressive strength of concrete. λ and k are adjustment factors for displacement ductility at shear failure and lightweight concrete, respectively, and are taken to be unity in this study. $\psi/100$ is the mass loss ratio, and β is the pitting coefficient that accounts for the influence of corrosion. Substituting Equations (3) and (4) into Equation (2) and rearranging terms results in the modified strength limit as shown in Equation (5)

$$V_{n\_cor} = C_v k\frac{A_v f_y d_b}{s} + \lambda k\left(\frac{6\sqrt{f_c'}}{\frac{M}{VD}}\sqrt{1+\frac{N_u}{6\sqrt{f_c'}A_g}}\right)0.8A_g \quad (5a)$$

$$C_v = 10(100-\psi)^{\frac{3}{2}}(1-\beta\psi) \quad (5b)$$

where C_v is the reduction factor that accounts for the corrosion effect. The strength limit curve is one of the thresholds that trigger shear degradation.

Next, the unloading stiffness is modified due to corrosion. Total displacement (Δ_{total}) of the system consists of contributions from the shear spring (Δ_s) and flexural element (Δ_f). As the shear spring and flexural element are connected in series, the total unloading stiffness (K_{deg}^t) is given in Equation (6) (Elwood, 2004).

$$K_{deg}^t = \left(\frac{1}{K_{deg}} + \frac{1}{K_{unload}}\right)^{-1} \tag{6}$$

K_{deg} is unloading stiffness of the shear spring and K_{unload} is unloading stiffness of the flexural element. Corrosion of reinforcement affects the shear spring's unloading stiffness, and therefore, on the total unloading stiffness. The unloading stiffness of the shear spring is a function of the maximum shear strength and the residual deformation (Δ_r) (LeBorgne, 2012), with residual deformation, computed based on the difference in shear deformation from the shear failure point to the point of zero shear force along the backbone as shown in Equation (7a). The residual drift ratio can be determined by clear column span (L) as in Equation (7b).

$$\Delta_r = -\frac{|V_n|}{K_{deg}} \tag{7a}$$

$$\frac{\Delta_r}{L} = -\frac{|V_n|}{K_{deg}L} \tag{7b}$$

The relation between the residual drift ratio and the column's multiple geometric and mechanical parameters is based on a stepwise regression shown in Equation (8).

$$\frac{\Delta_r}{L} = -0.16 - 15.4\rho_t - 0.009\frac{l_d}{d_b} + 0.7\frac{A_{cc}}{A_g} + 0.58\frac{f_y A_s}{f_c' A_g} \geq 0.02 \tag{8}$$

ρ_t is transverse reinforcement ratio, l_d is development length of longitudinal bars, A_{cc} is the gross confined area bounded by transverse reinforcement in the column section, and A_s is the total area of longitudinal reinforcement bars. To account for corrosion, Equations (7) and (8) is modified to

$$\frac{\Delta_{r\_cor}}{L} = -\frac{|V_{n\_cor}|}{K_{deg}^{cor} L} \tag{9}$$

$$\frac{\Delta_{r\_cor}}{L} = -0.16 - 15.4 C_t \rho_t - 0.009 C_b \frac{l_d}{d_b} + 0.7 C_{cc} \frac{A_{cc}}{A_g} + 0.58 C_y \frac{f_y A_s}{f_c' A_g} \geq 0.02 \tag{10}$$

where C_t, C_b, C_{cc}, and C_y are reduction factors for transverse reinforcement ratio, development ratio ($\frac{l_d}{d_b}$), confinement ratio ($\frac{A_{cc}}{A_g}$), and longitudinal steel distribution in column section ($\frac{f_y A_s}{f_c' A_g}$), respectively. Each of these corrosion reduction factors can be expressed in terms of mass loss (ψ) and pitting corrosion coefficient (β) as

$$C_t = 1 - \frac{\psi}{100} \tag{11a}$$

$$C_b = \frac{10}{\sqrt{100 - \psi}} \tag{11b}$$

$$C_{cc} = 1 \tag{11c}$$

$$C_y = 1 - \beta \psi \tag{11d}$$

Note that Equation (11c) is a unit under the assumption that corrosion has a minimal effect on the confinement ratio. From Equations (9) and (10), the corroded unloading stiffness of the shear spring (K_{deg}^{cor}) is expressed as shown in Equation (12).

$$K_{deg}^{cor} = -\frac{\left| C_v k \frac{A_v f_y d_b}{s} + \lambda k \left(\frac{6\sqrt{f_c'}}{\frac{M}{VD}} \sqrt{1 + \frac{N_u}{6\sqrt{f_c'} A_g}} \right) 0.8 A_g \right|}{\left(-0.16 - 15.4 C_t \rho_t - 0.009 C_b \frac{l_d}{d_b} + 0.7 C_{cc} \frac{A_{cc}}{A_g} + 0.58 C_y \frac{f_y A_s}{f_c' A_g} \right) L} \tag{12}$$

Assuming corrosion has a minimal effect on the unloading stiffness of the flexural element, the updated total unloading stiffness for a shear-critical column ($K_{deg}^{t\_cor}$) is

$$K_{deg}^{t\_cor} = \left(\frac{1}{K_{deg}^{cor}} + \frac{1}{K_{unload}} \right)^{-1} \tag{13}$$

The shear spring is triggered by reaching either the strength limit or plastic hinge rotation capacity. The force-displacement relation, shown in Figure 3, is for the scenario where the strength limit is the governing factor. This scenario represents either a pure shear failure in which shear degradation is triggered before yielding of longitudinal reinforcement takes place, or shear-flexure failure in which the column fails in shear with a certain level of flexural deformation. Corrosion also impacts the column's total unloading stiffness due to the residual drift change in the shear spring backbone curve.

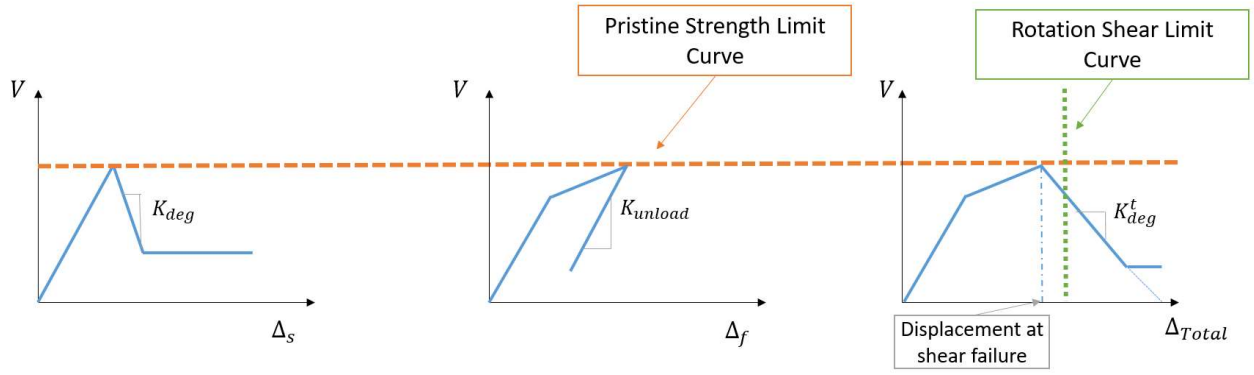

Figure 3. Force-displacement relation and effect of corrosion with shear spring controlled by strength limit curve

Another scenario is when shear degradation is triggered when the plastic hinge region's rotation reaches its limit. Physically, this typically represents shear-flexure failure. This study assumes that corrosion has

no impact on the rotational capacity across the plastic hinge at shear failure. Rotational capacity (θ_f) is computed based on Equation (14) obtained from a stepwise regression as in Leborgne (2012).

$$\theta_f = 0.027 - 0.033\frac{N_u}{A_g f_c^{'}} - 0.01\frac{s}{d} \geq 0.006 \quad (14)$$

s is transverse reinforcement spacing, and d is column depth.

The implementation of corrosion on the risk assessment of a bridge with a shear-critical column is presented later in this report. This is performed through seismic fragility assessment of a sample bridge consisting of a corroded shear-critical column. Results quantify the impact of corrosion on this failure mode in terms of increasing the probabilities of exceeding defined damage states.

3 COLUMNS WITH SHORT LAP SPLICE CONSIDERING CORROSION EFFECT

Many aging bridges with lap-sliced columns, including those with pre-1970s designs, include short starter bars and widely spaced transverse reinforcement in the bottom of the column. This study combines findings from several previous studies to model the behavior of lap-spliced columns. The mechanism transferring the tensile stress in the splice relies on the concrete tensile stress capacity. The concrete acts as an intermediate material that transfers forces between two adjacent bars (Priestley et al. 1996). This stress-transferring mechanism causes radially outward pressures on the concrete, leading to splitting cracks along the bars. Cracking the concrete in tension causes softening initiation due to the degrading behavior of lap-spliced reinforcement (Wight and MacGregor, 2009). In addition to inadequate lap-spliced length, light transverse reinforcement in the lap-spliced region reduces the column's ductility once the cover concrete has spalled.

3.1 Numerical model accounting for corrosion effects

To quantify the lap-spliced constitutive behavior, this work adopts the relations found in Priestley et al. (1996) to obtain the value of maximum stress and residual stress in the splice. Equations (15) and (16) show maximum force and stress developed in the lap-spliced region, respectively.

$$T_b = A_b f_s = F_t p l_{sp} \tag{15}$$

$$f_s = \frac{F_t p l_{sp}}{A_b} \tag{16}$$

T_b and f_s are force and stress developed in the lap-spliced bar, respectively, A_b is the cross-sectional area of the longitudinal bar, F_t is the tensile strength of concrete, l_{sp} is the length of the lap splice, and p is the perimeter of the cylindrical block, which is determined through Equation (17) with an upper limit for widely spaced spliced bars.

$$p = \frac{s}{2} + 2(d_b + c) \leq 2\sqrt{2(c + d_b)} \tag{17}$$

s is the average distance between lap-spliced bars, and c is the length of concrete cover. Once degradation has initiated, residual stress f_r is computed based on Equation (18) as proposed by Wight and MacGregor (2009).

$$f_r = \frac{\mu A_h f_s}{n A_b} \frac{l_{sp}}{S} \tag{18}$$

μ is a frictional factor, which is taken as 1.4, A_h is the cross-sectional area of transverse reinforcement, and n is the number of spliced bars. This study obtains strain at both peak stress and residual stress by Tariverdio et al. (2009), which assumes that displacement corresponding to maximum stress is 1 mm, and displacement corresponding to slip occurrence is 10 mm. Equation (19) shows the calculation of strain at peak stress.

$$\varepsilon_s = \frac{f_s}{E_s} + \frac{\Delta_{BarSlip}}{l_{ss}} \quad (19)$$

E_s is the elastic modulus of steel bar, $\Delta_{BarSlip}$ at peak stress is taken as 1 mm, and l_{ss} is the length in which displacement due to slip occurs. Figure 4(a) shows the material constitutive behavior of lap-spliced bar (Tariverdio et al., 2009).

Figure 4(b) shows the numerical beam-column model used to capture lap-spliced failure in this study. Similar to the model for a shear-critical column, the numerical model consists of two bond-slip elements located at the top and bottom of the column and a middle node to account for the inflection point at the column mid-span. However, unlike the shear-critical model with two beam-column elements, this model consists of an additional beam-column element at the column's bottom. The length of the bottom element is set to be equivalent to the length of the lap splice. Uniaxial fibers used in the bottom element constitute confined and unconfined concrete fibers and steel fibers with the lap-splice stress-strain model shown in Figure 4(a), which can account for degradation triggered by lap-splice failure.

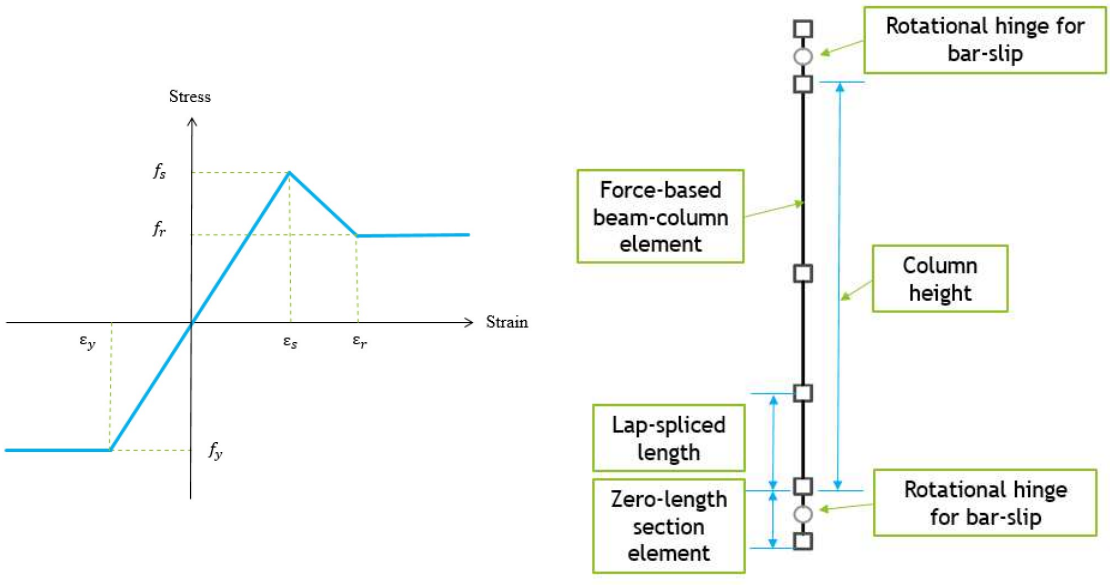

(a) (b)

Figure 4. (a) Constitutive material model of the lap-spliced bar (Tariverdio et al., 2009) and (b) numerical model for lap-spliced column

3.2 Verification with experimental tests

Results from the model are compared with outcomes from two experimental column tests to verify the numerical model of the lap-spliced column. Experimental data on corroded lap-spliced columns are not available, so results are compared with pristine columns. The first test specimen for comparison is from static cyclic tests conducted by Sun et al. (1993). The column has a rectangular cross section with a width of 730 mm and a height of 3.66 m. The lap splice length is 381 mm with longitudinal and transverse reinforcement ratios of 2.55% and 0.184%, respectively. The lap-spliced length is 20 times the diameter of the longitudinal bar. Numerical static cyclic test results (dashed line) compared to experimental results (solid line) from this specimen are shown in Figure 5(a). The numerical model can predict degradation in load-carrying capacity and capture the failure mode of the bond slip of lapped reinforcement.

The second test specimen is from tests conducted by Chail et al. (1991). The column is circular with a diameter of 610 mm and a clear height of 3.66 m. Longitudinal and transverse reinforcement ratios are 2.53% and 0.174%, respectively. The lap-spliced length is 381 mm, which is 20 times the diameter of the longitudinal bar. Numerical compared to experimental static cyclic test results for this specimen are shown in Figure 5(b). Comparing the numerical and experimental results, the numerical model can capture the load-carrying capacity degradation as demand increases.

Table 2 shows the percentage differences between the numerical and experimental results regarding peak force and displacement corresponding with a 20% strength drop. Most of the percentage differences are below 10%, except for the second specimen's displacement quantity with around a 16% difference. This discrepancy could be caused by measurement error during the experimental test or modeling error in terms of accuracy of the fiber uniaxial behavior and damage parameters accounting for

pinching behavior. However, with the other results, the numerical model is able to capture the force-displacement envelope of the lap-splice column with sufficient accuracy.

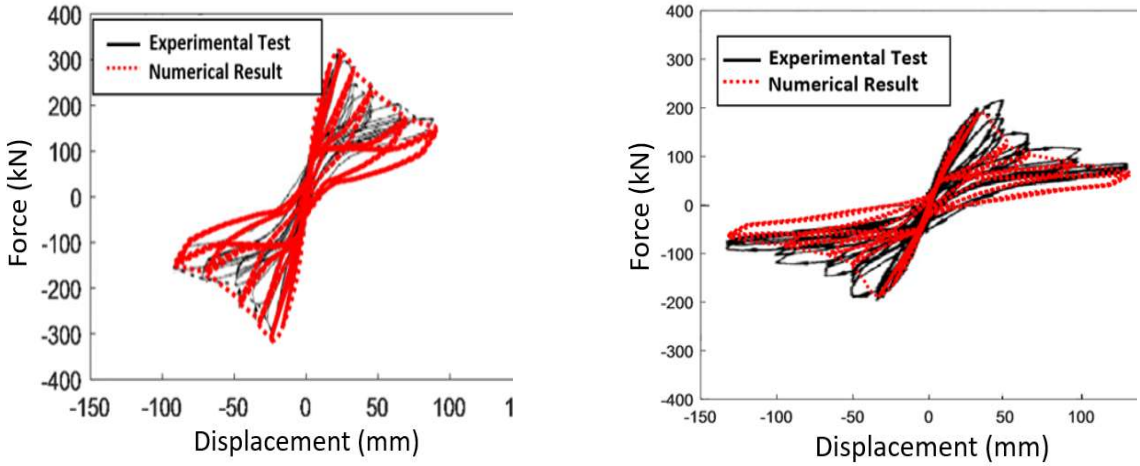

(a) (b)

Figure 5. Static cyclic curves comparing experimental test results from (a) Sun and Priestley (1993) and (b) Chail et al. (1991) with numerical results from this study

Table 2. Comparison between experimental tests and numerical model results for lap-spliced column

	Specimen 1		Specimen 2	
	Peak Force (kN)	Displ. at 20% Strength Drop (mm)	Peak Force (kN)	Displ. at 20% Strength Drop (mm)
Experimental Test	300	37.0	218	59.7
Numerical Model	318	39.0	198	50.1
% Difference	6.0%	5.4%	9.2%	16.2%

4 SEISMIC FRAGILITY ASSESSMENT

Before integrating the numerical models into a full bridge to perform fragility assessment, there are several steps to select the column type for the analysis, starting with the column's material and geometric information, influencing the failure mode. Figure 6 shows the flowchart for choosing the column type.

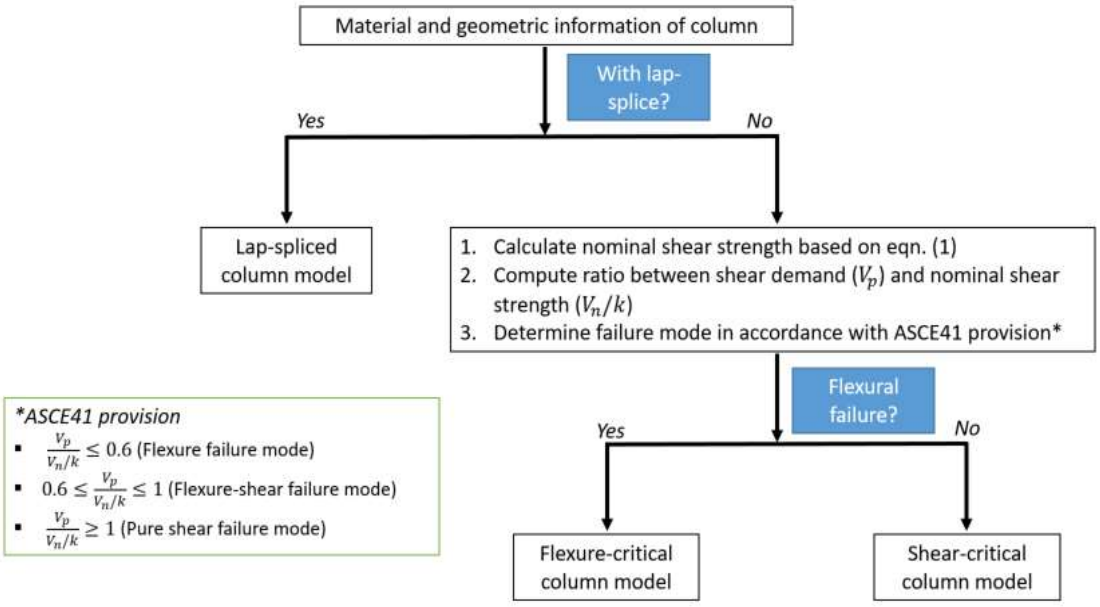

Figure 6. Flowchart for selecting an appropriate numerical model for bridge column

Note that the lap-spliced model presented in this work can predict the structural response of a column with both short lap splice (20-24 times d_b) and long lap splice. In other words, the lap-spliced column model is able to capture both pull-out failure and flexural failure. The shear-critical column model, shown in Figure 10, is able to capture both pure shear and flexure-shear failure modes.

4.1 Bridge parameters

A full bridge is studied to assess the impact of corrosion on fragility. The sample multi-continuous concrete single frame box girder bridge is shown in Figure 7. This bridge type is typically used for longer spans and

constitutes, for example, the bulk of the highway bridge inventory in California (Ramanathan, 2012). Table 3 summarizes the geometric parameters' median and dispersion values describing this bridge class built before 1971. These values and the corresponding distributions are used for the generation of fragility curves in this study. Values used for column diameter are 1.2 m, 1.5 m, and 1.8 m, and transverse spacing is 305 mm on center irrespective of the column size or reinforcement.

Table 3. Median values of geometric parameters used for fragility assessment

Geometric Parameters	Distribution Type	Median	Standard Deviation
Span length (L)	Lognormal	36.6 m	0.27 m
Deck width (Dw)	Lognormal	10.5 m	0.16 m
Column height (H)	Lognormal	6.8 m	0.12 m
Total depth of super-structure (h)	Lognormal	1.46 m	0.27 m
Longitudinal reinforcement ratio	Uniform	1.9 %	0.08 %

A finite-element model of this bridge is built in OpenSees. The column is modeled with fiber sections for the sub-structure, consisting of the appropriate uniaxial constitutive models for concrete and steel. This element type enables us to capture the spread of plasticity along the column. Uncertainty in material parameters includes the compressive strength of concrete and yield strength of Grade 60 reinforcement. The concrete compressive strength is modeled using a normal distribution with a mean of 5000 psi and a standard deviation of 627 psi (Choi, 2002). Yield strength is modeled as lognormally distributed with a median of 4.21 ksi and coefficient of variation 0.08 (Ellingwood and Hwang, 1985). The super-structure is modeled using equivalent elastic beam-column elements under the assumption that elements remain linear elastic during a seismic event. For the foundation system, translational and rotational springs are used to model pile-supported footings, including a pile cap and piles underneath, with foundation springs consisting of zero-length elements at the columns' base. Uncertainty in the bridge system's damping is modeled using a normal distribution with a mean of 0.045 and a standard deviation

of 0.0125 (Nielson, 2005; Padgett, 2007). Further details on the modeling of bridge components can be found in Ramanathan (2012).

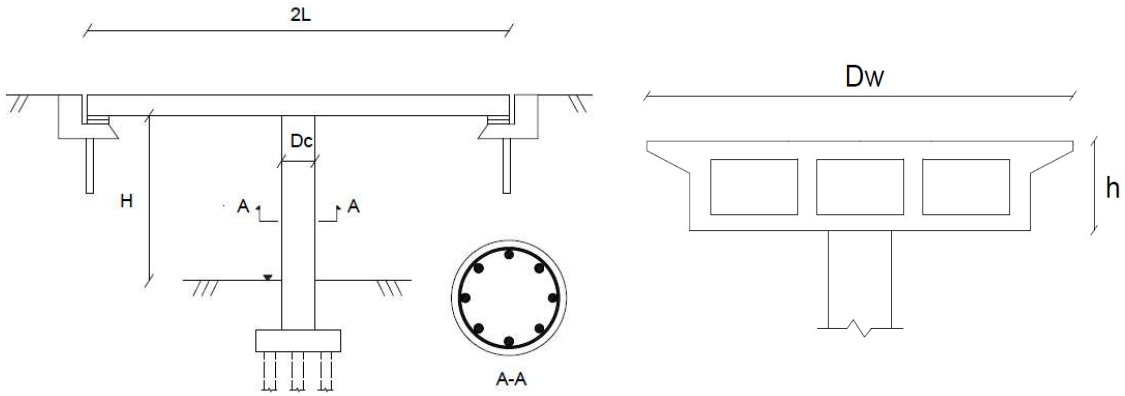

(a) (b)

Figure 7. (a) Longitudinal view and (b) transverse view of sample bridge

This study utilizes a suite of ground motions selected from the NGA-2 database for the fragility assessment. The selected ground motion suite consists of 320 ground motions developed to match California's hazard characteristics. The first 160 motions' median response is similar to that of the full 320-motion set; therefore, the first 160 ground motions are included in the analysis. The response spectra of the ground motions in the two horizontal directions are shown in Figure 8.

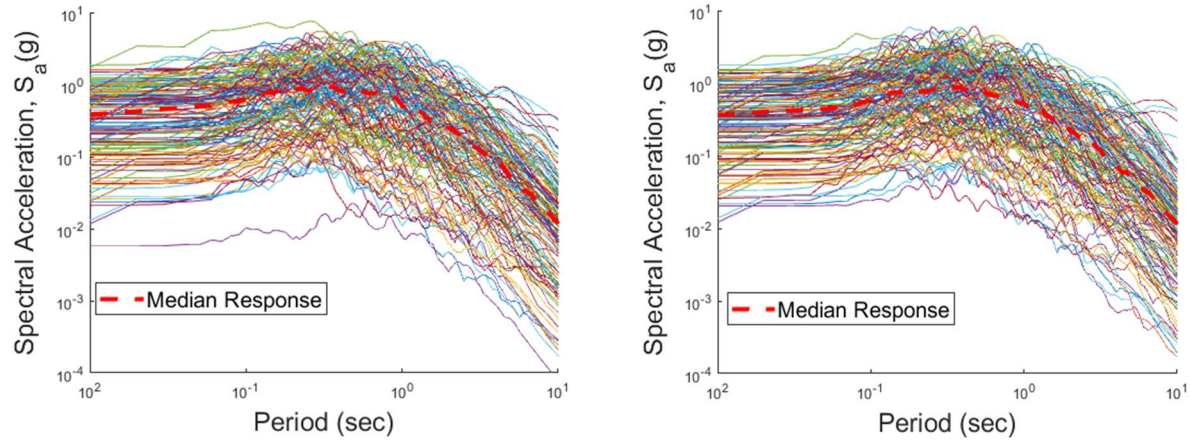

(a) (b)

Figure 8. Response spectra for the selected ground motions in (a) horizontal component one and (b) horizontal component two

4.2 Bridge risk assessment

To assess risk, analytical fragility curves are computed by running a series of nonlinear time history analyses (Shinozuka et al., 2000). This approach is chosen to account for the multiple sources of uncertainty present in the problem, including bridge geometries, material properties, and loading characteristics. In particular, the uncertainties considered in the analysis include the bridge geometry parameters shown in Table 3, as well as uncertainties in the top flange thickness, longitudinal reinforcement ratio, transverse reinforcement ratio, height of the abutment backwall, translational and rotational stiffness of foundation, concrete compressive strength, yield strength of reinforcing steel, the gap between the girder and the shear key, the gap between the deck and the abutment backwall, multiplication factor for deck mass, damping ratio, ground motions, and direction. Several previous studies have adopted this methodology for fragility assessment (Choi et al., 2004; Padgett, 2007; Pan et al., 2010; Ramanathan et al., 2012). However, these studies have not explicitly considered corrosion in shear-critical and lap-spliced columns to quantify this deterioration's effect on predicted bridge performance.

Risk is quantified based on calculated fragilities, where fragility is defined as in Equation (24), interpreted as the probability of exceeding a particular damage state given a specific ground motion intensity.

$$P_f = P[DS|IM = y] \tag{24}$$

P_f is the probability of exceedance, DS is damage state, IM is intensity measure of ground motion, and y is a realization of intensity measure. Equation (24) can also be expressed as a function of parameters of capacity and demand variables assuming both follow lognormal distributions as shown in Equation (25).

$$P_f = \Phi\left(\frac{\ln S_d/S_c}{\sqrt{\xi_d^2 + \xi_c^2}}\right) \quad (25)$$

S_d and S_c are the median parameters for the demand and capacity distributions, respectively, ξ_d and ξ_c are the lognormal standard deviation of the demand and capacity distributions, respectively, and $\Phi(\cdot)$ is the standard normal cumulative distribution function. The engineering demand parameter used for the fragility analysis is the displacement at the bridge column's mid-span.

Damage is discretized into four damage states, as shown in Table 4. A description of each damage state for shear-critical and lap-spliced columns is provided in terms of displacement ductility. As the damage state increases, the column undergoes more damage until it reaches a near collapse state (DS-4). Figure 9 and Figure 10 show fragility curves for the shear-critical and lap-spliced column, respectively. Fragility is a function of ground motion intensity as indicated by peak ground acceleration (PGA). Results provide probabilities of exceeding each damage state for columns with varying corrosion levels measured by percentage mass loss of reinforcement.

Table 4. Description of column damage states

Damage State	*Description*	*Shear-critical*	*Lap-spliced*
DS-1	Slight	Initial cracking	Initial cracking
DS-2	Moderate	Onset of diagonal cracking	Significant cracking
DS-3	Extensive	Significant diagonal cracking	Initial spalling
DS-4	Complete	Shear failure	Complete spalling/lap-splice failure

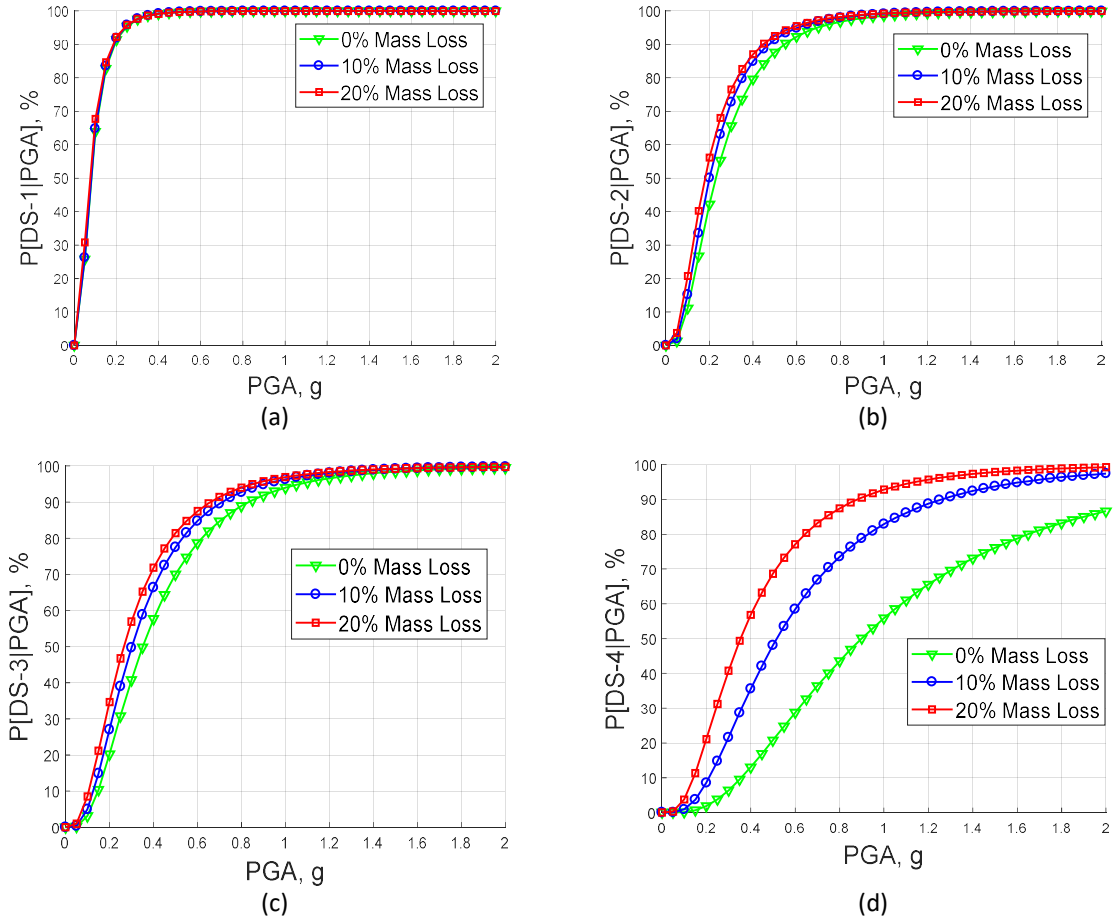

Figure 9. Fragility curves for probabilities of exceeding (a) DS-1, (b) DS-2, (c) DS-3, and (D) DS-4 for the shear-critical column with varying levels of corrosion

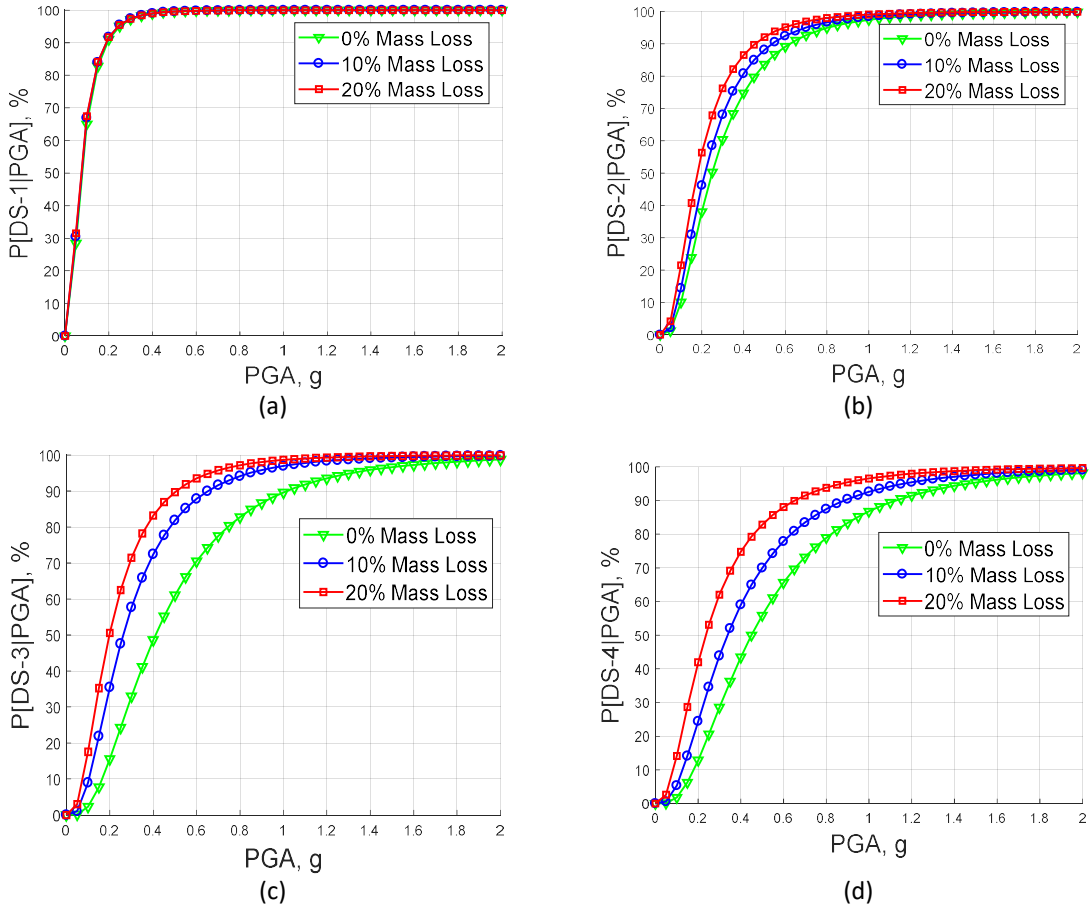

Figure 10. Fragility curves for probabilities of exceeding (a) DS-1, (b) DS-2, (c) DS-3, and (D) DS-4 for the column with short lap splice and varying levels of corrosion

From Figure 9 and Figure 10, corrosion has a minimal effect on both failure modes' initial damage state. As damage accumulates, however, the influence of corrosion increases, with larger increases in the probabilities of exceeding undesired damage states compared to the non-corroded state. This is mainly seen in DS-4 (near collapse state) for shear-critical bridges.

To better assess corrosion's influence, Figure 11 shows the difference in probability of exceeding DS-4 for each column type. The comparison is between the pristine state and the 10% mass loss and 20% mass loss corroded cases. This enables quantification of the increase in risk from corroded columns. From Figure 11, 20% mass loss increases the failure probabilities of a shear-critical column and lap-spliced

column by up to 49% and 34%, respectively. This indicates the importance of considering corrosion in assessing structural risk. At higher PGA values, the effect of increasing corrosion is less pronounced. This is because, under high-intensity loadings, structures are more likely to fail regardless of the structure's condition. Instead, there is uncertainty about the structure's performance in the intermediate loading intensities, and corrosion has a more significant effect.

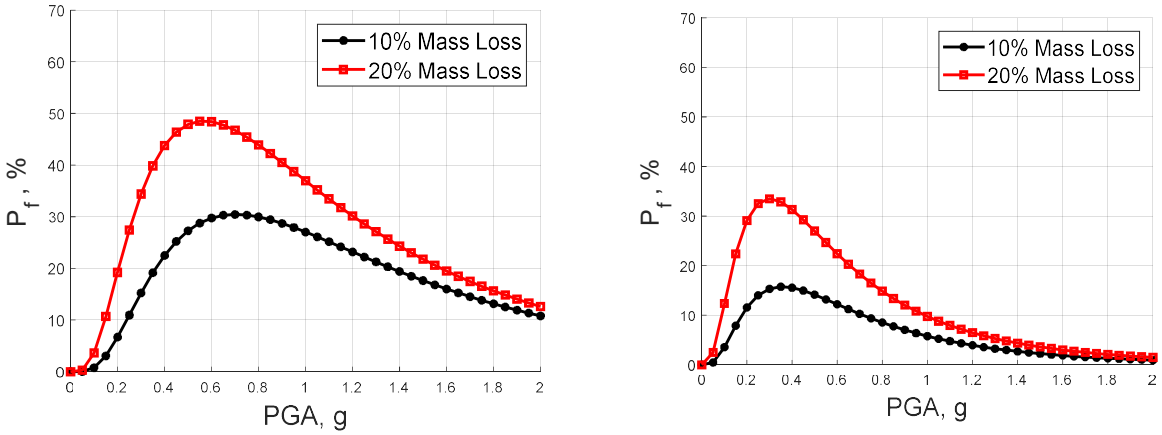

Figure 11. The difference in failure probability for DS-4 between the pristine state and varying corrosion levels for (a) shear-critical column and (b) lap-spliced column

Figure 12 shows the fragility curves for DS-4 for a shear-critical column and lap-spliced column to compare corrosion's effect across failure modes. Besides, the authors have previously investigated the fragility of flexure-critical columns for the same bridge type. These results are also provided in Figure 16 for comparison. The reader is referred to Zhang et al. (2018) for more details on the flexure-critical analysis. Figure 12 shows that lap-spliced columns are the most vulnerable at 10% mass loss, followed by shear-critical then flexure-critical columns. At 20% mass loss, lap-spliced columns remain the most vulnerable among the three. However, the difference between the three modes is less pronounced. At relatively low corrosion levels, the effect of corrosion on the shear-critical column is more extensive than

for flexure-critical because the shear-critical case experiences additional damage due to shear degradation. In comparison, at higher corrosion levels, the effect of further damage due to shear degradation becomes relatively less significant compared with the pure corrosion effect on the geometric and material properties of reinforcement, leading to changes in column performance. Thus, flexure-critical columns' failure probability becomes close to that of shear-critical columns at the higher corrosion level.

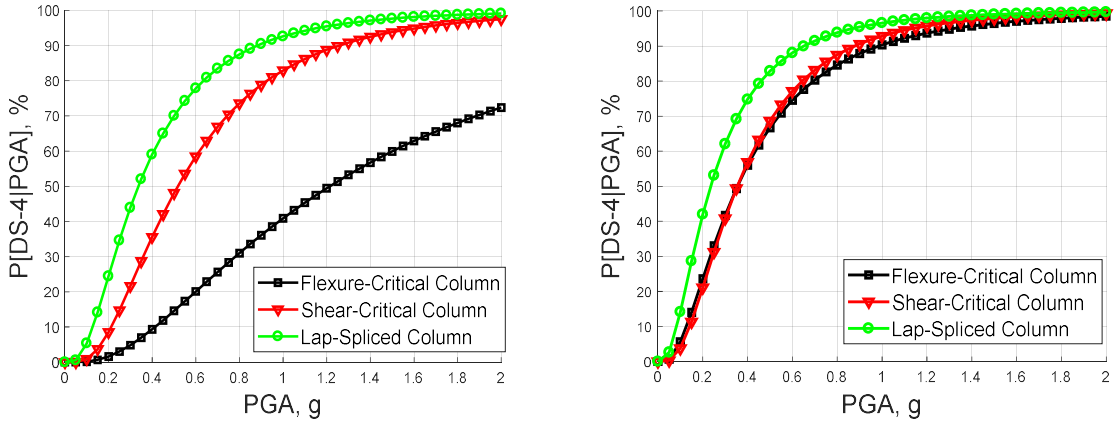

(a) (b)

Figure 12. Fragility curves for DS-4 considering different failure modes with corrosion levels of (a) 10% mass loss and (b) 20% mass loss

5 CONCLUSIONS

In this project, a methodology to account for corrosion's effect on low-ductility columns' predicted performance, such as shear-critical columns and columns with short lap splices, was presented. Corrosion's effects include reducing the amount of longitudinal and transverse reinforcement and weakening the bond strength between steel and concrete through corrosion-induced cracking (Zhang et al., 2019).

For shear-critical columns, corrosion decreases the shear capacity with reduced contribution from the transverse reinforcement. With the reduced shear strength limit, the column undergoes early shear degradation, eventually leading to brittle shear failure. For columns with short lap splice, corrosion causes volumetric expansion of reinforcement, generating tensile stress on the surrounding concrete. Consequently, cracking of concrete cover leads to bond deterioration and loss of the force transferring mechanism between the concrete and reinforcement in the lapped region. This reduces the column load-carrying capacity, leading to pull-out failure.

With these effects accounted for, corrosion's impact on bridges' predicted performance with shear-critical and short lap-spliced columns was analyzed. This was done through conducting analytical fragility assessments. Results quantify the increases in probabilities of the bridge exceeding given damage states with increasing levels of corrosion. The results show corrosion having a larger effect for more severe damage states and at intermediate loading intensities. Twenty percent mass loss of column reinforcement increases the probability of exceeding the complete damage state by up to 49% and 34% for a shear-critical and lap-spliced column, respectively. Moreover, columns with short lap splice are more vulnerable to collapse under the same corrosion attack level than shear-critical columns. The results demonstrate a methodology to update assessments of bridge risk based on collected corrosion inspection data.

6 REFERENCES

ACI (American Concrete Institute). (2011). Building code requirements for structural concrete and commentary.

Almusallam, A. A. (2001). Effect of degree of corrosion on the properties of reinforcing steel bars. *Construction and Building Materials*, *15*(8), 361-368.

American Society of Civil Engineers (ASCE). (2007). *Seismic rehabilitation of existing buildings*, ASCE/SEI 41-06. Reston, VA: American Society of Civil Engineers.

Ang, B. G. (1985). Seismic shear strength of circular bridge piers.

Apostolopoulos, C. A., Papadopoulos, M. P., & Pantelakis, S. G. (2006). Tensile behavior of corroded reinforcing steel bars BSt 500s. *Construction and building materials*, *20*(9), 782-789.

Chail, Y. H., Priestley, M. N., & Seible, F. (1991). Seismic retrofit of circular bridge columns for enhanced flexural performance. Structural Journal, 88(5), 572-584.

Choi, E. (2002). *Seismic analysis and retrofit of Mid-America bridges*, Ph.D. thesis, School of Civil and Environmental Engineering, Georgia Institute of Technology, Georgia.

Choe, D., Gardoni, P., Rosowsky, D., & Haukaas, T. (2009). Seismic fragility estimates for reinforced concrete bridges subject to corrosion. Structural Safety, 31, 275–283.

Du, Y. G., Clark, L. A., & Chan, A. H. C. (2005). Effect of corrosion on ductility of reinforcing bars. *Magazine of Concrete Research*, *57*(7), 407-419.

Ellingwood, B. R., Hwang, H. (1985). *Probabilistic Descriptions of Resistance of Safety-Related Structures in Nuclear Plants*, Nuclear Engineering and Design, 88(2), 169-178.

Elwood, K. J. (2004). Modelling failures in existing reinforced concrete columns. *Canadian Journal of Civil Engineering*, *31*(5), 846-859.

FHWA, U. (2013). National bridge inventory. *US FHWA*.

Ghosh, J., & Padgett, J. E. (2010). Aging considerations in the development of time-dependent seismic fragility curves. *Journal of Structural Engineering*, *136*(12), 1497-1511.

Kashani, M. M., Crewe, A. J., & Alexander, N. A. (2013). Use of a 3D optical measurement technique for stochastic corrosion pattern analysis of reinforcing bars subjected to accelerated corrosion. *Corrosion Science*, *73*, 208-221.

Kashani, M. M., Lowes, L. N., Crewe, A. J., & Alexander, N. A. (2015). Phenomenological hysteretic model for corroded reinforcing bars including inelastic buckling and low-cycle fatigue degradation. *Computers & Structures*, *156*, 58-71.

Kashani, M. M., Lowes, L. N., Crewe, A. J., & Alexander, N. A. (2016). Computational modelling strategies for nonlinear response prediction of corroded circular RC bridge piers. *Advances in Materials Science and Engineering*, *2016*.

LeBorgne, M. R. (2012). *Modeling the post shear failure behavior of reinforced concrete columns* (Doctoral dissertation).

LeBorgne, M. R., & Ghannoum, W. M. (2013). Analytical element for simulating lateral-strength degradation in reinforced concrete columns and other frame members. *Journal of Structural Engineering*, *140*(7), 04014038.

Liu, K. Y., Witarto, W., & Chang, K. C. (2015). Composed analytical models for seismic assessment of reinforced concrete bridge columns. *Earthquake Engineering & Structural Dynamics*, *44*(2), 265-281.

McKenna, F. T. (1997). *Object-oriented finite element programming: frameworks for analysis, algorithms and parallel computing*. (Doctoral dissertation). Berkeley, CA: University of California at Berkeley.

Nielson, B. G. (2005). *Analytical Fragility Curves for Highway Bridges in Moderate Seismic Zones*, Ph.D. Dissertation, Georgia Institute of Technology, Atlanta, GA.

Padgett, J.E. (2007). *Seismic vulnerability assessment of retrofitted bridges using probabilistic methods*, Ph.D. Dissertation. Georgia Institute of Technology, Atlanta, GA.

Pan, Y., Agrawal, A.K., Ghosn, M., & Alampalli, S. (2010). Seismic fragility of multi-span simply supported steel highway bridges in New York State. I: Bridge modeling, parametric analysis, and retrofit design. ASCE Journal of Bridge Engineering, 15, 448–461.

Priestley, M. N., Seible, F., Calvi, G. M., & Calvi, G. M. (1996). *Seismic design and retrofit of bridges*. John Wiley & Sons.

Ramanathan, K. N. (2012). *Next generation seismic fragility curves for California bridges incorporating the evolution in seismic design philosophy* (Doctoral dissertation, Georgia Institute of Technology).

Shinozuka, M., Feng, M.Q., Kim, H.-K., & Kim, S.-H. (2000). Nonlinear static procedure for fragility curve development. ASCE Journal of Engineering Mechanics, 126, 1287–1296.

Sun, Z., Priestley, M. J. N., & Seible, F. (1993). *Diagnostics and retrofit of rectangular bridge columns for seismic loads*. Department of Applied Mechanics & Engineering Sciences, University of California, San Diego.

Tariverdilo, S., A. Farjadi, and M. Barkhordary. (2009). "Fragility Curves for Reinforced Concrete Frames With Lap-Spliced Columns." *International Journal of Engineering - Transactions A: Basics* 22 (3): 213.

Wight, J. K., & MacGregor, J. G., (2009). Reinforced concrete: mechanics and design (Fifth ed.). New Jersey: Prentice Hall Upper Saddle River, NJ.

Zhang, Y., DesRoches, R., & Tien, I. (2019). Impact of corrosion on risk assessment of shear-critical and short lap-spliced bridges. *Engineering Structures*, *189*, 260-271.

Zhao, J., & Sritharan, S. (2007). Modeling of strain penetration effects in fiber-based analysis of reinforced concrete structures. *ACI structural journal*, *104*(2), 133.